8. Bykov A A et al. *Pis'ma Zh. Eksp. Teor. Fiz.* **74** 182 (2001) [*JETP Lett.* **74** 164 (2001)]
9. Entin M V, Magarill L I *Phys. Rev. B* **64** 085330 (2001)
10. Entin M V, Magarill L I *Phys. Rev. B* **66** 205308 (2002)
11. Magarill L I, Éntin M V *Zh. Eksp. Teor. Fiz.* **123** 867 (2003) [*JETP* **96** 766 (2003)]
12. Chaplik A V, Blick R H *New J. Phys.* **6** 33 (2004)
13. Chaplik A V *Pis'ma Zh. Eksp. Teor Fiz.* **80** 140 (2004) [*JETP Lett.* **80** 130 (2004)]

PACS numbers: 72.15.Gd, 72.15.Rn, **73.63.–b**, 73.63.Bd, 73.63.Fg
DOI: 10.1070/PU2005v048n09ABEH005733

Heterogeneous electronic states in carbon nanostructures with different dimensionalities and curvatures of the constituent graphene layers

A I Romanenko, A V Okotrub, V L Kuznetsov, A S Kotosonov, A N Obraztsov

1. Introduction

Production of skeleton carbon nanostructures is always accompanied by curving the constituent graphene layers. New properties result that are not characteristic of the graphite composed of the plane graphene layers. The most brightest display of graphene layer-curvature is the existence of a superconducting state in the bundles of single-layer carbon nanotubes 10 Å in diameter (with the radius of curvature $r = 5$ Å) at the temperature $T_c \sim 1$ K [1], and the presence of superconductivity in nanotubes 4 Å in diameter ($r = 2$ Å) at $T_c = 16$ K [2], whereas no superconducting transition is observed in graphite. None the less, Y Kopelevich et al. [3] stated that superconductivity in an ideal graphite must show itself and that in real graphite samples superconductivity was not observed due to omnipresent defects. It is our belief that superconducting state in skeleton carbon nanostructures is related to curvatures of graphene layers forming them.

In addition, the crystal structures of nanocrystallites, for instance, nano-onions, not only have curved surfaces but also have one-dimensional fibres of various lengths and curvatures [4]. This results in reduced dimensionalities of motion of charge carriers in such structures.

This report is concerned with experimental determination of the electron–electron interaction constant λ_c in carbon nanostructures based on curved graphene layers, and with the peculiarities of motion of charge carriers in systems composed of curved surfaces and one-dimensional fibres.

2. Methods of investigation

The general method of studying the electron–electron interaction constant has been a combined analysis of the quantum corrections to the electrical conduction, magnetic conductance and magnetic susceptibility of the investigated samples. All graphene-layer-based skeleton nanostructures usually possess structural defects resulting in charge carrier diffusion at low temperatures. The quantum corrections to kinetic and thermodynamic quantities due to quantum interference are therefore observed in them at a low enough temperature. For single-particle processes (localization effects, LEs [5, 6]), this is the interference of wave functions of an electron proceeding along the closed trajectories in opposite directions (for path lengths l smaller than the phase interruption length $L_\varphi(T) = (D\tau_\varphi)^{1/2}$, where D is the diffusion coefficient, and τ_φ is the phase interruption time). As a consequence, the full conductance decrease: when the temperature decreases, $L_\varphi(T)$ grows and the conductance goes down.

In a magnetic field, the additional phase shift of various signs are added, depending on the direction round of closed trajectory. The interference is therefore suppressed provided that $L_B = (\hbar c/2eB)^{1/2} < L_\varphi$, resulting in a negative magnetoresistance (NMR) — that is, the conductance increases in a magnetic field. Electron–electron interaction effects (IE) [7] also produce quantum corrections. In this case, at a repeat interaction of two electrons at distances less than the interference length $L_{\rm int} = (D\hbar/k_{\rm B}T)^{1/2}$ ($L_{\rm int}$ is the distance through which information about the electron phase change in the course of previous interaction have not yet lost), the repeat interaction will depend on their previous one. The effective density of states $\nu_{\rm F}$ on the Fermi surface therefore proves to be renormalized. The interaction effects contribute not only to electrical conduction, but also to the thermodynamic quantities dependent on $\nu_{\rm F}$, namely, the magnetic susceptibility χ, and the heat capacity. Contrary to corrections to electrical conduction and magnetoresistance, the corrections to thermodynamic quantities are due to EC effects only.

To determine the effective dimensionality of motion of the charge carriers, we have used combined analysis of temperature dependences of electrical conduction and magnetoresistance in the conditions of variable range hopping conduction.

3. Arc-produced multiwall carbon nanotubes

A distinguishing feature of multiwall carbon nanotubes (MWNTs) that were produced at the Institute of Inorganic Chemistry, SB RAS [8, 9] with an electric-arc technology is the presence of nanotube bundles preferentially oriented in a plane perpendicular to the electric arc axis, therefore the MWNT-based bulk samples possess an anisotropy of electrical conductivity: $\sigma_{||}/\sigma_\perp \sim 100$ [8, 9], where $\sigma_{||}$ is the electrical conductivity in the plane of the preferred orientation of nanotube bundles, and $\sigma_\perp$ is the electrical conductivity in the direction normal to this plane. The mean diameter of a single nanotube is $d \sim 140$ Å. According to the electron paramagnetic resonance data, our samples contain less than 10^{-6}% of paramagnetic impurities, thus excluding the impurity contribution to the susceptibility observed. Bromination of MWNTs in bromine vapors at room temperature [9] produces a sample of $CBr_{0.06}$ chemical composition and results in a conductivity increase due to the higher concentration of hole (p-type) charge carriers. The corrections to orbital susceptibility $\delta\chi_{\rm orb}$ in the Cooper channel were theoretically predicted [7] to be the main contributors to quantum corrections to magnetic susceptibility $\chi(T, B)$ in the magnetic fields below $B_c = (\pi k_{\rm B}T/g\mu_{\rm B})^{1/2}$ ($B_c = 9.8$ T at $T = 4.2$ K). These corrections are determined by the value and sign of the electron–electron interaction constant λ_c and are proportional to the diamagnetic susceptibility $\chi_{\rm orb}$ of electrons. Since the diamagnetic susceptibility of graphites and multiwall carbon nanotubes is greater than that of any

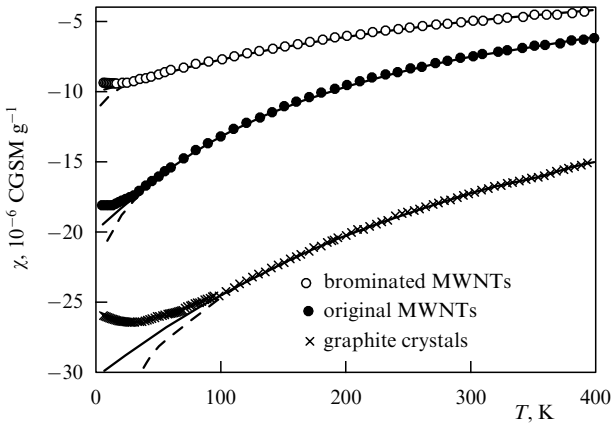

Figure 1. The temperature dependences of the magnetic susceptibility $\chi(T)$ of arc-produced MWNTs and graphite crystals, measured in magnetic field $B = 0.01$ T. Solid lines depict regular parts of $\chi(T)$.

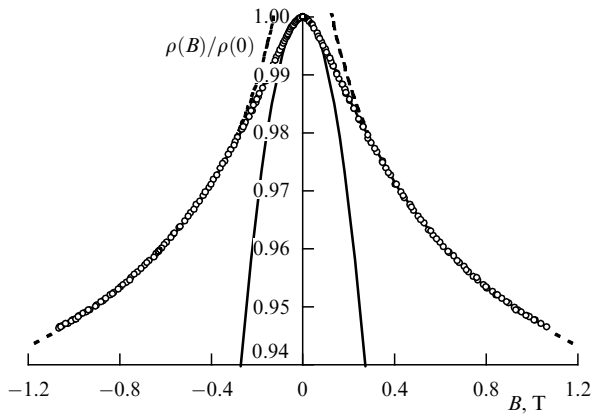

Figure 2. The relative magnetoresistivity $\rho(B)/\rho(0)$ of arc-produced MWNTs, measured at $T = 4.2$ K. The solid line depicts a quadratic asymptotics $\rho(B)/\rho(0) \sim B^2$. Dashed lines represent a logarithmic asymptotics $\rho(B)/\rho(0) \sim \ln(T)$.

other nonmagnetic materials (besides superconductors), then the correction $\chi_{\rm orb}$ must also be the major one.

Figure 1 shows the dependences of the magnetic susceptibility $\chi(T)$ of the initial MWNTs, the brominated MWNTs and graphite crystals on temperature. The solid lines represent the regular parts of $\chi(T)$, obtained by approximating the experimental data in the framework of a model [10] for magnetic susceptibility of quasi-two-dimensional graphites. The model also well describes the experimental findings for MWNTs [10]. At temperatures below 50 K, the experimental data are observed to deviation from the approximation curve. The deviation observed occurs in the direction of greater susceptibility [11, 12]: $\delta\chi(T) = \chi(T)_{\rm exp} - \chi(T)_{\rm appr} > 0$, where $\chi(T)_{\rm exp}$ fits the experimental data, and $\chi(T)_{\rm appr}$ fits the experimental data approximated by the theoretical dependence for quasi-two-dimensional graphites in the 50–400 K temperature range. According to theory [7], this means that the electron–electron interaction constant is positive, i.e., electrons are repulsed from one another. In the case of attraction, the susceptibilities would drop (dashed lines in Fig. 1). The theoretical approximation of the anomalous part of magnetic susceptibility has revealed the following three features.

I. As the magnetic field grows, the two-dimensional corrections at $B = 0.01$ T cross over with the three-dimensional ones at $B = 5.5$ T for MWNTs and brominated MWNTs. At the same time, three-dimensional corrections to $\chi(T, B)$ are observed for graphite at any field intensity. This is related to the fact that the magnetic length $L_B = (\hbar c/2eB)^{1/2} = 77$ Å at $B = 5.5$ T becomes comparable to the thickness h of the graphene layers composing MWNTs, whereas in the magnetic field of $B = 0.01$ T one finds $L_B = (\hbar c/2eB)^{1/2} = 1800$ Å $\gg h$, but is shorter than the tube length l ($l \sim 1$ μm). In graphite, the graphene-layer package thickness is always a macroscopic quantity and is larger than any characteristic length.

II. Bromination of the MWNT samples resulted in a 10-fold increase in their conductivity (from 500 Ω^{-1} cm^{-1} in MWNTs to 5000 Ω^{-1} cm^{-1} in brominated MWNTs). At the same time, the relative correction to magnetic susceptibility, $\delta\chi(T)/\chi(T)$, that determines the value of $\lambda_{\rm c}$ remains the same. Bromination, therefore, does not change the electron–electron interaction constant $\lambda_{\rm c}$ in arc-produced multiwall carbon nanotubes.

III. The value of constant $\lambda_{\rm c} \sim 0.2$ [10] is greater for MWNTs and brominated MWNTs than for graphite, where $\lambda_{\rm c} \sim 0.1$ [11], i.e., the curvature of MWNT graphene layers leads to the increase in $\lambda_{\rm c}$.

The analysis of the temperature dependences of electrical conduction and magnetoresistance also revealed the presence of quantum corrections to electrical conduction and the negative magnetoresistance of MWNTs. But it is quite problematic to extract the EC contribution in the Cooper channel, determined by the value and sign of $\lambda_{\rm c}$, against the background of LEs and EC effects in the diffusion channel. As the magnetoresistance data show (see Fig. 2), the LE-related negative magnetoresistance dominates in the whole range (0–1 T) of the field intensities used. All three mechanisms contribute to the quantum corrections to electrical conduction. Therefore, in order to extract the EC contribution in the Cooper channel, it is necessary to get rid of the LE contribution to the greatest possible extent. We succeeded in doing this when using catalytic multiwall carbon nanotubes synthesized by a special technology which excludes the presence of carbon impurities from the side of carbon not entering into the composition of nanotubes.

4. Catalytic multiwall carbon nanotubes

Paramagnetic impurities are always present in catalytic MWNTs since ferromagnetic metals are used as catalysts. Therefore, due to the major contribution of the paramagnetic impurities at low temperatures, the information about $\lambda_{\rm c}$ cannot be extracted from the data on magnetic susceptibility of catalytic MWNTs. We have conducted a more thorough analysis of the resistivity data to which a considerably smaller contribution is made by paramagnetic impurities. Drawn in Fig. 3 are the graphs of the relative magnetoresistivity $\rho(B)/\rho(0)$ for MWNTs obtained by a conventional catalytic method [13] (full circles) and by a special technique [14] permitting the production of MWNTs practically without amorphous carbon impurities (open circles). From a comparison of the graphs one can see that, contrary to the EL-related contribution to negative magnetoresistance in conventionally produced catalytic nanotubes [15, 16], the LE-related contribution to negative magnetoresistance in weak magnetic fields is absent in purified samples. For purified catalytic

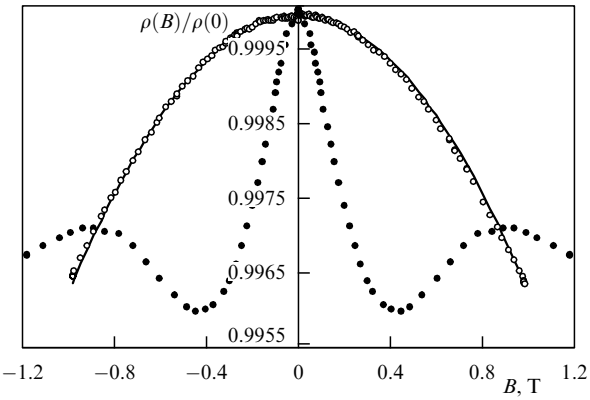

Figure 3. Relative magnetoresistivity $\rho(B)/\rho(0)$ of catalytically produced MWNTs, measured at $T = 4.2$ K: ○ — MWNTs obtained by a special technique excluding the presence of impurities: • — conventional MWNTs. The solid line depicts a quadratic asymptotics $\rho(B)/\rho(0) \sim B^2$.

MWNTs, the relative magnetoresistivity $\rho(B)/\rho(0)$ is given by a quadratic dependence $\rho(B)/\rho(0) \sim B^2$, which is the asymptotics of the EC-related negative magnetoresistivity at low field intensities $B < 1$ T. The study of $\sigma(T)$ of catalytic MWNTs has revealed quantum corrections conforming to $\delta\sigma(T) \sim \ln(T)$, which points to their two-dimensional character [5–7]. The magnetic field suppressing the temperature correction $[\delta\sigma(4.2\text{ K})/\sigma(4.2\text{ K}) \sim 27\,\%]$ is estimated to be $B \sim 8.5$ T, and it corresponds to a rather reasonable value for the magnetic length $L_B = (\hbar c/2eB)^{1/2} \sim 60$ Å. The presence of negative magnetoresistance for EC also agrees with the conclusion that $\lambda_c > 0$. But it is the resistivity data that have given this result.

5. Carbon films containing graphite-like nano-sized crystallites

For our investigations, carbon nanofilm samples have been precipitated on a silicon substrate from a methane – hydrogen gaseous mixture activated by a direct current discharge [17]. The top layer of the film is made of thin graphite-like crystallites with thickness d ranging from 15 to 150 Å, resembling crumbled paper sheets up to 1–3 μm in height attached to the middle layer grains. All crystallites contact each other, thus forming an intermittent irregular reticular structure drawing an electric current. The $\sigma(T)$ curves are plotted in Fig. 4. The departure of the experimental curve $\sigma(T)_{\text{exp}}$ (circles) from the regular part $\sigma(T)_{\text{extr}}$ (solid line) is given by the relationship $\delta\sigma(T) = \sigma(T)_{\text{exp}} - \sigma(T)_{\text{extr}} \sim \ln(T)$ (see inset to Fig. 4) pointing to two-dimensionality of quantum corrections [5–7]. It is related to the fact that typical lengths L_φ and L_{int} are larger than d. A similar curve for graphite is given in Fig. 5 for comparison. The observed relationship $\delta\sigma(T) \sim T^{1/2}$ (see inset to Fig. 5) points to the three-dimensional nature of the quantum corrections to electrical conductivity [5–7], as is the case for the magnetic susceptibility [11]. The study of magnetoresistivity in the graphite crystals showed the dominance of LE-related negative magnetoresistivity.

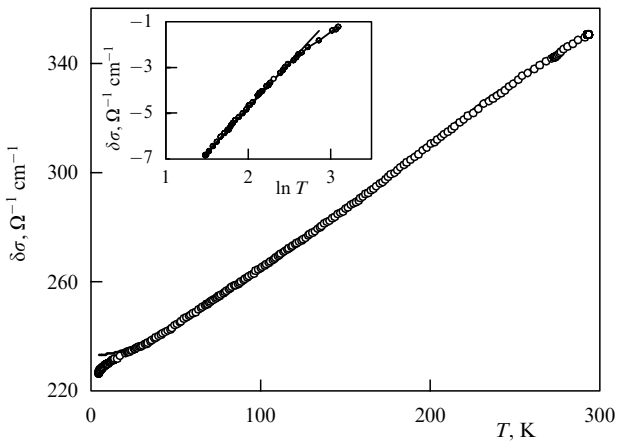

Figure 4. The temperature dependence $\sigma(T)$ of electrical conductivity, measured in a film involving carbon nano-sized crystallites. The solid line represents the regular part of $\sigma(T)$. The anomalous part of the temperature dependence of conductivity, $\delta\sigma(T)$, obtained by subtraction of the regular part from the experimental data, is shown in the inset.

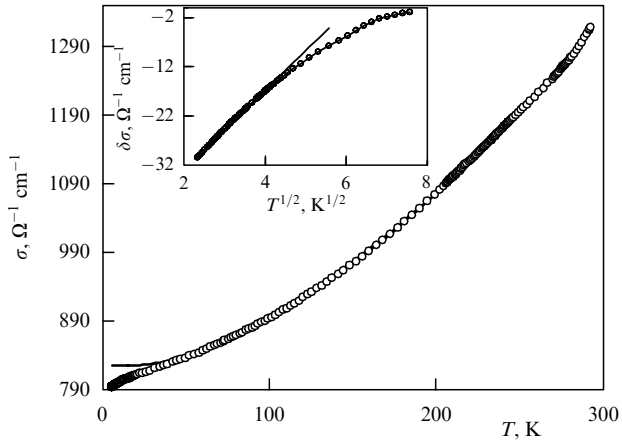

Figure 5. The measured temperature dependence $\sigma(T)$ of a graphite crystal conductivity. The solid line represents the regular part of $\sigma(T)$. The anomalous part of the temperature dependence of conductivity, $\delta\sigma(T)$, obtained by subtraction of the regular part from the experimental data, is shown in the inset.

6. Onion-like carbon

Onion-like carbon (OLC) samples were prepared from fine diamond by annealing at temperatures of 1800 K, 1900 K, and 2140 K [4]. The samples obtained were mainly composed of multiwall defect spheres ('onions') measuring $d_{\text{oni}} \sim 50$ Å across, with distances between the layers inside the spheres being ~ 3.5 Å, which corresponds to quasi-two-dimensional graphite layer spacing. These spheres form agglomerates size 500–5000 Å. A bulk powdered sample is comprised of such agglomerates. For taking measurements, the powder was poured into a cylindrical ampoule with four silver contacts. Electrical resistance of the samples thus prepared was measured with the four-probe method.

The temperature dependence of the OLC electrical resistivity (inset to Fig. 6) is typical for the case of variable range hopping [18] and is given by the relationship $\rho(T) = \rho_0 \exp(-T_0/T)^\alpha$. It best approximates the experimental data when $\alpha = 1/2$ at the intermediate annealing temperature of 1900 K, and $\alpha = 1/3$ at annealing temperatures of 1800 K and 2140 K. One-dimensional carbon fibres generated during diamond graphitization at the intermediate stage (1900 K) are several dozen angstroms long (a of about

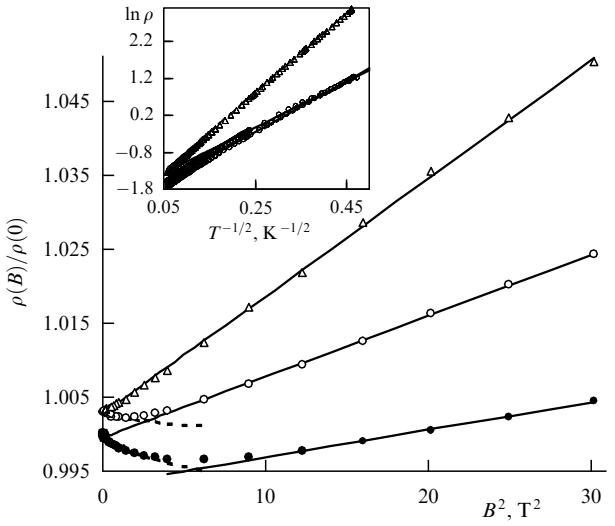

Figure 6. Relative magnetoresistivity $\rho(B)/\rho(0)$ of diamond-graphitization-prepared OLCs, measured at $T = 4.2$ K. The OSCs were prepared at following annealing temperatures: ○ — $T_{\rm ann} = 1800$ K; • — $T_{\rm ann} = 2140$ K, and △ — $T_{\rm ann} = 1900$ K. Quadratic asymptotics $\rho(B)/\rho(0) \sim B^2$ are shown by solid lines, and the dependences $\ln[\rho(T,B)/\rho(T,0)] \sim -A\{(eB/\hbar c)\,n^{-2/3}\}\ln[\rho(T)/\rho_0]$ are given by dashed lines. The temperature dependences of electrical resistivity of the same samples are plotted in the inset (ρ is measured in [Ω cm]).

chain 10 carbon atoms in length). The dependence with $\alpha = 1/2$ appears to be due to one-dimensional variable range hopping, like that of carbines [19]. Further nanodiamond graphitization brings these fibres together in curved graphene layers and a dependence with $\alpha = 1/3$ due to two-dimensional variable range hopping is observed.

The graphs of relative magnetoresistivity $\rho(B)/\rho(0)$ measured at $T = 4.2$ K are portrayed in Fig. 6. For $B > 3$ T, positive magnetoresistivity is given by the relationship $\Delta\rho(B)/\rho(0) \approx (l/r_{\rm L})^2$, where l is the electron mean free path, $r_{\rm L} = cv_{\rm F}m/(eB)$ is the Larmor radius, and $v_{\rm F}$ is the velocity of an electron on a Fermi surface. Assuming $v_{\rm F} \sim 1.5 \times 10^7$ cm s^{-1}, $m \sim 0.07m_{\rm e}$, l is estimated to be $l \sim 12$ Å for a sample annealed at 1800 K, $l \sim 80$ Å for a sample annealed at 1900 K, and $l \sim 18$ Å for a sample annealed at 2140 K [20–22]. A nonmonotonous variation of l ($l \sim d_{\rm oni}$ at the annealing temperature 1900 K) points to the practically imperfection-free structure of such onions. The spheres forming them mainly consist of a multiply connected mesh made of linear carbine chains. At field intensities $B < 3$ T, negative magnetoresistance (see Fig. 6)of samples annealed at the first (1800 K) and the third (2140 K) stages is observed and is also related to quantum corrections [23].

In a magnetic field, the threshold concentration $n_{\rm c}$ of the charge carrier localization is theoretically predicted [23] to shift lower, resulting in an electrical conduction increase, i.e., in negative magnetoresistance. In samples annealed at the intermediate stage (1900 K), the imperfections inside the onions are practically absent and negative magnetoresistance is not observed. Using the negative magnetoresistance data obtained in experiment we estimated the relative change in charge carrier concentration n in OLCs in the context of the negative magnetoresistance theory for the conditions of variable range hopping with $\ln\left[\rho(T,B)/\rho(T,0)\right] = -A\left\{(eB/\hbar c)\,n^{-2/3}\right\}\ln\left[\rho(T)/\rho_0\right]$ [23]. The resulting charge carrier concentration in a sample annealed at 1800 K proved to be three-fold higher than that in a more graphitized sample annealed at 2140 K [20–22]. This finding is in agreement with the fact that in skeleton carbon structures the charge carrier concentration grows in the presence of imperfections.

7. Conclusions

The analysis of the anomalous part of magnetic susceptibility, $\delta\chi(T)$, below 50 K made possible the estimation of the electron–electron interaction constant $\lambda_{\rm c}$ for arc-produced multiwall carbon nanotubes ($\lambda_{\rm c} \sim 0.2$) and for graphite ($\lambda_{\rm c} \sim 0.1$). A change in concentration of charge carriers by bromination of arc-produced MWNTs has been shown not to affect $\lambda_{\rm c}$. The analysis of the anomalous part of electrical conductivity and of negative magnetoresistance points to the dominance of the contributions of localization effects to electrical conductivity and negative magnetoresistance.

Negative magnetoresistance of impurity-free catalytic MWNTs was discovered. It is related to electron coupling effects only, pointing to positive sign of $\lambda_{\rm c}$ in these nanotubes.

The quasi-two-dimensional quantum corrections to electrical conductivity and negative magnetoresistance have been discovered in films composed of graphite nano-sized crystallites, which is in full agreement with the crystallites' thickness h being smaller than L_φ and $L_{\rm int}$ ($h \sim 15-150$ Å). Three-dimensional quantum corrections to electrical conduction and negative magnetoresistance were discovered in macroscopic graphite crystals, since in such crystals h is always greater than L_φ and $L_{\rm int}$.

Variable range hopping and nonmonotonous change in electrical conduction with nanodiamond graphitization were discovered in onion-like carbon. Samples annealed at the intermediate temperature (1900 K) have the lowest conductivity and one-dimensional variable range hopping. Two other samples annealed at 1800 K and 2140 K were found to have two-dimensional hopping and negative magnetoresistance. From negative magnetoresistance data, the charge carrier concentration was estimated to be highest in a sample with the most defects at the initial stage of graphitization (annealing temperature $T_{\rm ann} = 1800$ K).

Thus, the analyses of temperature and field dependences of magnetic susceptibility, magnetoresistance, and electrical conductivity of heterogeneous systems make possible the estimation of the electron–electron interaction constant $\lambda_{\rm c}$ and finding the effective dimensionality of motion of the charge carriers. In skeleton carbon nanostructures, graphene layer distortion leads to a change in $\lambda_{\rm c}$.

This work was supported by RFBR grants Nos 03-02-16458 and 05-03-32901, by the interdisciplinary "Integration" program of SB RAS (grant No. 113), by the program "Development of the Science Potential of Higher Education" (grant No. 8234), by the "Universities of Russia" program (UR.01.01.186), and by a joint grant of CRDF and the RF Ministry of Education (No. 008-X1).

References

1. Kociak M et al. *Phys. Rev. Lett.* **86** 2416 (2001)
2. Tang Z K et al. *Synthetic Met.* **133–134** 689 (2003)
3. Kopelevich Y et al. *Physica C* **408–410** 77 (2004)
4. Kuznetsov V L et al. *Chem. Phys. Lett.* **336** 397 (2001)
5. Kawabata A *Solid State Commun.* **34** 431 (1980)
6. Lee P A, Ramakrishnan T V *Rev. Mod. Phys.* **57** 287 (1985)
7. Al'tshuler B L, Aronov A G, Zyuzin A Yu *Zh. Eksp. Teor. Fiz.* **84** 1525 (1983) [*Sov. Phys. JETP* **84** 1525 (1983)]

8. Okotrub A V et al. *Appl. Phys. A* **72** 481 (2001)
9. Romanenko A I et al. *Fiz. Tverd. Tela* **44** 634 (2002) [*Phys. Solid State* **44** 659 (2002)]
10. Kotosonov A S, Kuvshinnikov S V *Phys. Lett. A* **230** 377 (1997)
11. Romanenko A I et al. *Solid State Commun.* **121** 149 (2002)
12. Romanenko A I et al. *Physica C* **388 – 389** 622 (2003)
13. Kudashov A G et al. *Fiz. Tverd. Tela* **44** 626 (2002) [*Phys. Solid State* **44** 652 (2002)]
14. Couteau E et al. *Chem. Phys. Lett.* **378** 9 (2003)
15. Kudashov A G et al. *Fullerenes Nanotubes Carbon Nanostruct.* **12** 93 (2004)
16. Romanenko A I et al., in *The Progresses in Function Materials: 11th APAM Conf. Proc., Ningbo, P. R. China, 2004*, p. 59
17. Zolotukhin A A et al. *Zh. Eksp. Teor. Fiz.* **124** 1291 (2003) [*JETP* **97** 1154 (2003)]
18. Mott N F, Davis E A *Electronic Processes in Non-crystalline Materials* 2nd ed. (Oxford: Clarendon Press, 1979)
19. Demishev S V et al. *Pis'ma Zh. Eksp. Teor. Fiz.* **78** 984 (2003) [*JETP Lett.* **78** 511 (2003)]
20. Romanenko A I et al. *Fiz. Tverd. Tela* **44** 468 (2002) [*Phys. Solid State* **44** 487 (2002)]
21. Romanenko A I et al. *Mater. Res. Soc. Symp. Proc.* **703** 259 (2002)
22. Okotrub A V et al., in *Electronic Properties of Molecular Nanostructures* (AIP Conf. Proc., Vol. 591, Eds H Kuzmany et al.) (Melville, NY: AIP, 2001) p. 349
23. Al'tshuler B L, Aronov A G, Khmel'nitskii D E *Pis'ma Zh. Eksp. Teor. Fiz.* **36** 157 (1982) [*JETP Lett.* **36** 195 (1982)]

PACS numbers: 03.65.Ge, 03.65.Nk, **73.63.–b**
DOI: 10.1070/PU2005v048n09ABEH005748

A generalized adiabatic principle for electron dynamics in curved nanostructures

V V Belov, S Yu Dobrokhotov, V P Maslov, T Ya Tudorovskii

1. Introduction

Progress in nanotechnology has made possible the production of extended thin quasi-one-dimensional and quasi-two-dimensional structures of complex geometries, namely, nanotubes and nanofilms. In our model, these structures are the areas of the thin bent 'twisted-edge' cylinder type or of the thin curved film type. Beyond these areas, the wave function $\Psi(\mathbf{r}, t)$ of a quantum particle either drops exponentially (a soft wall model) or equals zero (a hard wall model). As in Refs [1, 2], we assume that the electron (three-dimensional) quantum dynamics in nanostructures in a magnetic field is given by the so-called Rashba Hamiltonian

$$\widehat{\mathcal{H}} = \frac{\widehat{\mathbf{P}}^2}{2m} + v_{\text{int}}(\mathbf{r}) + v_{\text{ext}}(\mathbf{r}, t) - \frac{e\hbar}{2mc}\,\langle \boldsymbol{\sigma}, \mathbf{H}\rangle + \widehat{\mathcal{H}}_{\text{so}}\,. \quad (1)$$

Here, $\mathbf{r}$ is the radius vector of a point in three-dimensional space; $\widehat{\mathbf{P}} = -\mathrm{i}\hbar\nabla - (e/c)\mathbf{A}(\mathbf{r}, t)$; e is the electron charge; m is the effective mass of a quasiparticle; $v_{\text{int}}(\mathbf{r})$ is the confinement potential; v_{ext}, $\mathbf{A}$ are the external field potentials; $\mathbf{H}(t) = \operatorname{rot}\mathbf{A}(\mathbf{r}, t)$ defines a homogeneous magnetic field; $\boldsymbol{\sigma} = \{\sigma_1, \sigma_2, \sigma_3\}$ are the Pauli matrices, and $\widehat{\mathcal{H}}_{\text{so}} = \alpha\langle\boldsymbol{\sigma}, [\nabla v_{\text{int}}, \widehat{\mathbf{P}}]\rangle$ is the operator for the interaction of the electron spin with the crystal electric field, with α constant being dependent on the given crystal type [3]. In the case of $v_{\text{int}}(\mathbf{r}) = 0$ and a zero wave function at the tube or film boundaries, we get 'empty structure' models. d and l_0 stand for the characteristic thickness and linear dimensions (e.g., tube length), respectively, of a tube or a film. In extended thin nanostructures, the scale difference may be conveniently characterized by a small 'adiabatic' parameter $\mu = d/l_0 \ll 1$. We restrict ourselves to the case of a weak enough magnetic field, thus considering the Larmor frequency $\omega_H = e|\mathbf{H}|/(mc) \sim \hbar/(mdl_0)$, and magnetic length $l_H \sim \sqrt{dl_0}$.

The Schrödinger nonstationary equation for electron quantum states $\Psi(\mathbf{r}, t)$ (including stationary ones) acquires the form

$$\mathrm{i}\hbar\Psi_t = \widehat{\mathcal{H}}\,\Psi\,. \quad (2)$$

We limit our consideration to a quantum particle (electron) in such tubes and films with slowly changing geometric characteristics, whose small segments with linear scales of order close to their thicknesses d may be quite accurately considered a right cylinder and a flat layer, respectively. It is clear that the effective electron dynamics in such structures have to be one- or two-dimensional and be represented by the equation with the effective Hamiltonian $\hat{L}^{\nu}$ for the wave function ψ^{ν} on the tube axis or the film surface:

$$\mathrm{i}\hbar\psi^{\nu}_t = \hat{L}^{\nu}\psi^{\nu}\,, \quad (3)$$

where ν is the number of a 'dimensional quantization subband'. To go over from Eqn (2) to Eqn (3), we use the procedure in which the function Ψ for the lower subbands with $\nu \ll \mu^{-1}$ is retrieved for ψ^{ν} by the action of 'intertwining' operator on ψ^{ν} (see Section 3.1). In stationary problems, the derivative $\mathrm{i}\hbar\partial/\partial t$ is substituted by the energy E.

Different characteristic dimensions and the presence of free carriers make possible the consideration of nanostructures as quantum waveguides or confined quantum systems [6 – 15]. Similar problems related to waveguides emerge in electrodynamics, acoustics, the theory of elasticity, marine physics, and so forth. Confinement elimination leading to lower system dimensionality is usually done by applying the adiabatic approximation equivalent to asymptotic partitioning of oscillations into longitudinal and transverse modes. For the Helmholtz equation, this partitioning was done in Ref. [16]. In that work, equation (3) for a longitudinal mode was given and it was shown that single-mode bound-state resonators may be made by varying the waveguide curvature [17]. Analogous equations for quantum-mechanical problems have been subsequently deduced in Refs [1, 2, 7 – 15]. It should be emphasized that the waveguide problems are similar to those of molecular physics, with the role of confinement potential being played by the Coulomb potential with 'frozen' coordinates of heavy nuclei. In mathematical literature, equations emerging in problems with different scales are called the operator-valued symbol equations [19].

The longitudinal-state wave functions ψ^{ν} can be: (1) delocalized and significantly changing on the scale of order l_0; (2) delocalized and rapidly oscillating, i.e., changing on the scale of $\lambda_{\parallel} \ll l_0$, and (3) asymptotically localized in the small sections with scales $\ll l_0$. We characterize the rate of the wave function change by a 'quasiclassical' parameter $h = \lambda_{\parallel}/l_0$, where $\lambda_{\parallel} = \max|\partial\psi^{\nu}/\partial x|^{-1}$ is the wavelength characteristic of ψ^{ν}. The final expressions for Ψ are significantly dependent on the relationships among $\lambda_{\parallel}$, d, and l_0 or, equivalently, on the relationship between the parameters μ and h.